Available online at www.sciencedirect.com
ScienceDirect
Catalysis Today 133–135 (2008) 383–393
CATALYSIS TODAY
www.elsevier.com/locate/cattod

Synthesis, characterization and catalytic behaviour of NiMgAl mixed oxides as catalysts for hydrogen production by naphtha steam reforming

F. Melo *, N. Morlanés

Instituto de Tecnología Química, UPV-CSIC, Avda. los Naranjos s/n, 46022 Valencia, Spain

Available online 28 January 2008

Abstract

NiMgAl mixed oxides obtained by thermal decomposition of layered double hydroxides have been studied in the reaction of hydrocarbon steam reforming for producing hydrogen. The effect of synthesis parameters such as method of introduction of active species, amount of components and thermal treatments (calcination and reduction) on structure and reactivity of these materials has been elucidated. Samples have been characterized by N_2 adsorption (BET), X-ray diffraction (XRD), temperature programmed reduction (TPR) and elemental analysis. Synthesis parameters have an important influence on metal–support interaction, when stronger are metal–support interactions more favourable is the catalyst structure for obtaining highly and finely dispersed nickel particles. Catalyst performance was strongly related to the nickel particle size. The support and its properties seem to play a key role in the performance of the hydrotalcite-derived catalysts.

Keywords: Steam reforming; Mixed oxides; Nickel intrinsic activity; Synthesis variables

1. Introduction

During the last three decades there are growing concerns about the shortage in energy supply in the world [1–3]. In order to solve this problem, hydrogen offers a potentially non-polluting and efficient fuel for today's rising energy demands with the development of fuel cell technology [4–6]. However, hydrogen must to be produced through conversion of hydrogen-rich energy carriers [7,8]. So, in the transition period before renewable sources of hydrogen can be developed, production of hydrogen from fossil fuels remains an important technology. For the transition to a hydrogen economy, it is important the development of an effective and efficient fuel processing technology from existing liquid fuels such as gasoline and diesel [9–11].

Hydrocarbon steam reforming is an important process for hydrogen production. Steam reforming process transforms a liquid hydrocarbon stream into a gaseous mixture constituted by CO_2, CO, CH_4 and H_2. The main reactions that take place are the following ones:

$$C_nH_m + nH_2O \rightarrow nCO + (n + 1/2m)\,H_2 \qquad \Delta H > 0 \qquad (1)$$

$$CO + 3H_2 \leftrightarrow CH_4 + H_2O \qquad \Delta H = -206\,\text{kJ/mol} \qquad (2)$$

$$CO + H_2O \leftrightarrow CO_2 + H_2 \qquad \Delta H = -41.2\,\text{kJ/mol} \qquad (3)$$

Steam reforming reaction takes place on the surface of a solid catalyst. For this process usually nickel supported catalysts are used. Water adsorbs preferentially on the catalysts support, formulated to allow mobility for oxygen species, originated from water dissociation, adsorbed on its surface, while hydrocarbon molecules adsorb preferentially on the metal surface (metallic nickel), and the steam reforming reaction takes place at the metal–support interface [12–16].

The low-cost and long-proven performance of Ni-based catalysts, therefore, warrants the efforts to optimize these catalysts for more demanding steam reforming applications [17–20]. Current research efforts have focused on catalyst development to improve activity, selectivity and stability under a realistic range of operating conditions. Generally, excess steam/carbon ratios of 4–6 are used to prevent coke formation but minimal water input is necessary to be considered to provide a higher hydrogen concentration.

* Corresponding author.
E-mail address: fmelo@itq.upv.es (F. Melo).

0920-5861/$ – see front matter © 2007 Elsevier B.V. All rights reserved.
doi:10.1016/j.cattod.2007.12.070

Carbon formation, which is the main disadvantage of steam reforming process, is a kinetic issue; it will depend on the relative rate of the possible carbon species reaction alternatives [21]. Process could take place through a mechanism or another one and it will depend on hydrocarbon type, operation conditions, and catalyst characteristics, which can play an important role in increasing selectivity towards the preferred reaction. To prevent carbon deposits, catalyst characteristics can influence [22] by increasing water adsorption-dissociation rate on the catalyst and gasification rate with respect to the C-C scission.

Catalyst characteristics are determined by their physical-chemistry, structural and textural properties, as they are: active area, metal particle size, metal dispersion and reducibility. These properties depend on metal–support interaction, and they could be established on different stages of catalyst synthesis. For example, varying precursor material composition, preparation method and/or heat treatments (calcination, reduction) [23–26].

Mixed oxides obtained by layered double hydroxides (LDHs) thermal decomposition [27–30] offer the opportunity to control the active site nature and its environment, as well as catalyst texture and stability. Thermal treatments lead to synergetic effects between the elements in mixed oxide structures, and after appropriate activation treatment, give rise to well dispersed metal particles like a supported metal catalysts, with the possibility of controlling metal–support interaction during the synthesis stages.

In the present work, we have studied nickel mixed oxide obtained by means of thermal decomposition of LDHs, and the behaviour of these materials on hydrocarbon steam reforming reaction. This work reports synthesis, physicochemical characterization and catalytic testing of three-element mixed oxides obtained by different preparation procedures and varying several synthesis parameters. The synthesis parameters studied are Al/Mg ratio, calcination and reduction temperature and method of nickel introduction on the structure (co-precipitation with magnesium and aluminium or impregnation on Al-Mg support). We have studied the effect of synthesis parameters on structure and reactivity of these materials in the mentioned reaction.

2. Experimental

2.1. Catalysts synthesis

Several materials LDH-type have been prepared by the precipitation method. Two solutions are prepared [31]. The acid solution contains nitrates of magnesium, nickel and aluminium with a desired $[Al^{3+}/(Ni^{2+} + Mg^{2+} + Al^{3+})]$ ratio and with a total concentration of $(Ni^{2+} + Mg^{2+} + Al^{3+}) = 1.5$ M. Whereas the basic solution is obtained mixing suitable amounts of NaOH with Na_2CO_3 that allow to maintain the relation $[CO_3^{2-}/(Ni^{2+} + Mg^{2+} + Al^{3+})] = 0.66$ and a pH of synthesis of 13. Solutions are added simultaneously into a bottle with mechanical agitation during 4 h. The obtained gel ages in propylene bottles at 333 K during 12 h, then the solid is filtered and washed with distilled water until the pH reaches neutral value (pH 7). Finally, the LDH material is dried at 333 K during 14 h and calcined in air up to 923 K during 6 h obtaining a mixed oxide Ni/Mg/Al. Supported metal catalysts suitable for steam reforming reaction are obtained from these precursors after reduction step. The activation of the materials is realized with a mixture 20% molar H_2 on N_2 to 1073 K during 1 h.

Synthesis parameters studied are:

- Al/Mg ratio: Al/(Al + Mg) = 0–1,
- calcination temperature: 298–1173 K,
- reduction temperature: 773–1073 K,
- nickel incorporation method: co-precipitation with magnesium and aluminium or impregnation on Al-Mg support.

In order to study the synthesis parameter effects on catalytic characteristics of these materials, different series of samples have been prepared. In each one we have varied only one of the parameters.

As base material, named 15-HT, we have considered that one synthesized with the following parameter values:

- nickel content: 15 wt.%,
- cation ratio: Al/(Al + Mg + Ni) = 0.25,
- calcination temperature: $T_c = 923$ K,
- reduction temperature: $T_r = 973$ K,
- nickel incorporation method: co-precipitation with magnesium and aluminium.

To determine aluminium/magnesium ratio effect on catalytic activity several catalysts have been prepared varying Al/(Al + Mg) between 0 and 1. These catalysts have been named *X*-HT-*Y*, where *X* indicates nominal nickel content (wt.%) and *Y* indicates Al/(Al + Mg) ratio.

To determine calcination temperature effect on catalytic activity several catalysts have been prepared varying calcination temperature between 723 and 1173 K. These catalysts have been named *X*-HT-c*Y*, where *X* indicates nickel content (wt.%) and *Y* indicates calcination temperature (K).

To determine reduction temperature effect on catalytic activity several catalysts have been prepared varying reduction temperature between 873 and 1073 K. These catalysts have been named *X*-HT-r*Y*, where *X* indicates nickel content (wt.%) and *Y* indicates reduction temperature (K).

To determine nickel incorporation method effect on catalytic activity: on one hand, several catalysts have been prepared by co-precipitation with different nickel content (5–20 wt.%) and the rest of variables as base catalyst; on the other hand, several catalysts have been prepared by impregnation different nickel contents on a magnesium/aluminium support prepared with the same parameters as base catalyst. These catalysts have been named *X*-HT-y, where *X* indicates nominal nickel content (wt.%) and y indicates nickel incorporation method (co-precipitation y = p, impregnation y = i).

2.2. Catalysts characterization

The materials (calcined, reduced and used for catalytic measurements samples) have been characterized by several

techniques in order to correlate catalytic activity results with their structural properties.

Chemical composition of calcined samples was determined by atomic absorption spectrophotometry using a Varian Spectra A-10 Plus apparatus. Samples were first dissolved in acid solutions (a mixture of HCl and HNO_3), and diluted to concentrations within the detection range of the instrument.

N_2 adsorption isotherms were obtained for calcined samples at 77 K over all range of relative pressures, using a Micromeritics ASAP 2000 automatic device on samples previously out gassed at 423 K for 12 h. BET specific areas were calculated from these isotherms using the BET method.

X-ray powder diffractograms were recorded for calcined, reduced and used samples, following the step-scanning procedure (step size 0.02°, 2θ scanning from 5° to 70°) using a Phillips X'pert diffractometer (monochromatized Cu Kα radiation, $\lambda = 0.15418$ nm). The average particle size for different phases present on each state of the sample (calcined, reduced or used) was estimated by Scherrer equation [32] using the most intense reflexion (nickel oxide: $2\theta = 43.3°$ of calcined samples diffractograms, and metallic nickel: $2\theta = 51°$ of reduced samples diffractograms).

Nickel area has been estimated (Eq. (4)) by means of a proposed equation on literature [33] that considers nickel particle size, nickel content on the sample and reduction degree reached on the activation stage.

$$A_{Ni} = \frac{5 \times 10^4 X_{Ni} \alpha_{Ni}}{\gamma_{Ni} d_{Ni}} \quad (4)$$

where A_{Ni}: nickel active area (m^2/g_{cat}); X_{Ni}: nickel content of the sample (g_{Ni}/g_{cat}); α_{Ni}: reached reduction degree ($g_{Ni}{}^{\circ}/g_{Ni}$); γ_{Ni}: nickel specific density, 8.9 g/cm^3; d_{Ni}: nickel particle size (Å) and 5×10^4: geometric factor taking into account nickel particle geometry.

Ni° metal dispersion can be estimated using equation (5) proposed on the literature [34], which has into account Ni° particle size and assumes spherical geometry of the metal particles with uniform site density.

$$D = \frac{971}{d_{Ni}} \quad (5)$$

where D: nickel metal dispersion (%) and d_{Ni}: nickel particle size (Å).

The reducibility of the calcined samples was studied by temperature-programmed reduction in Micromeritics Autochem 2910 equipment, using a thermal conductivity detector in order to determine H_2 consumption. From temperature programmed reduction (TPR) curves, temperature at which a maximum in the curve appears (nickel reduction temperature), has been used like a nickel–support interaction degree measurement, being it more intense when higher is that temperature. Reduction degree has been estimated comparing temperature programmed reduction curves corresponding to calcined and reduced samples.

Coke formation on samples during activity tests has been determined by elemental analysis in an Elemental Analyzer CE1110, model CHNS.

2.3. Catalytic activity measurements

Steam reforming reaction study is carried out in a down-flow fixed-bed catalytic system, designed for this purpose, which allows comparing different catalysts and reaction conditions, with the aim of optimizing hydrogen production.

Hydrocarbon feed is composed by a mixture of *n*-heptane and *n*-hexane (in a weight ratio $C_7/C_6 = 2$) simulating a naphtha. Water and hydrocarbon feed are introduced mixed with a proportion of nitrogen and hydrogen. Nitrogen is used as carrier gas and as internal pattern for gas analysis. Hydrogen is used to avoid nickel oxidation on reduced samples. Molar proportion of reactant mixture is hydrocarbon/H_2O/H_2/N_2: 4/82/10/2.

Activity tests were performed using 0.25 g of catalyst (0.25–0.42 mm particle size) diluted with SiC (0.42–0.60 mm particle size) at a volume ratio of 1:10 to avoid adverse thermal effects.

The samples in their reduced form are tested in the naphtha steam reforming process. Operation conditions studied are: $P = P_{atm}$, $T = 823$ K, $S/C = 3H_2O$ mol/atom C, $W/F = 2$ g_{cat}·h/hydrocarbon mol, $G_{total}HSV = 225{,}160\ h^{-1}$. Prior to reaction the catalysts were reduced in situ with 20 vol.% H_2/N_2 mixture.

The catalyst bed is placed in a stainless-steel reactor ($d_i = 10$ mm, $l = 400$ mm) with several coaxially centred thermocouples. During the reaction the temperature in the catalyst bed is maintained and controlled by means of three independent heating zones with the corresponding temperature controllers.

The reaction products are analyzed on-line by gas chromatography. The gas chromatograph is constituted by two independent channels, equipped each one of them with a thermal conductivity detector. First channel allows to separate CO_2, CO, CH_4 and N_2; and the second one allows separate hydrogen from the rest of constituents.

In order to compare catalytic activity for different catalysts, several tests have been made at the same operation conditions (pressure, temperature, steam/carbon ratio and contact time) and we have measured hydrocarbon conversion at the 45 min of reaction time. From hydrocarbon conversion we have calculated nickel intrinsic activity defined as mol of hydrocarbon converted per hour and per nickel surface in square meter (Eq. (6)), and we have compared intrinsic activity for all synthesized catalysts.

$$\text{nickel intrinsic activity} = \frac{\text{hydrocarbon mol converted}}{m^2_{Ni} \cdot \text{hour}} = \frac{X_{HC}}{(W/F) \cdot A_{Ni}} \quad (6)$$

where: X_{HC}: hydrocarbon conversion (%); W/F: contact time (g_{cat}·h /hydrocarbon mol); A_{Ni}: nickel active area (m^2/g_{cat}).

In order to compare catalyst resistance to carbon deposition we have compared the carbon content present on used samples

analyzed by elemental analysis of different samples exposed at reaction conditions during the same period of time (8 h).

We have studied intrinsic activity and carbon deposition resistance as catalytic characteristics presented by these materials, since selectivity to different products is determined by thermodynamic equilibrium between gaseous species according to operation conditions at which this process takes place (pressure, temperature, steam/carbon ratio and space velocity) and it was studied in a previous work [35].

3. Results and discussion

In order to correlate activity results with structural characteristics of the catalysts we must take into account several mechanism considerations. Reaction mechanism, proposed by Rostrup Nielsen [16–19], establishes that hydrocarbon molecules are adsorbed on a dual site on catalyst surface where nickel selectively attacks terminal carbon of the chain by means of successive α-scission steps. Water adsorbs preferentially on the catalysts support, that must be formulated to allow mobility for oxygen species (which proceed from water dissociation) adsorbed on its surface, and the steam reforming reaction takes place, preferentially, at the metal–support interface. The C_1 species formed can react with oxygen species coming from water adsorption-dissociation and spill-over from support to nickel active sites [16], or remain adsorbed on the active sites where they would be transformed according to one of the possible carbon formation routes. We can outline this sequence:

Hydrocarbon adsorption-dissociation:

$$C_nH_m + 2* \rightarrow C_nH_z - *2 + (m-z)/2\,H_2 \quad (7)$$

C-Cα-scission:

$$C_nH_z - *2 + n* \rightarrow C_{n-1}H_z' - *2 + CH_x - *n \quad (8)$$

Steam adsorption-dissociation:

$$H_2O + \text{sup} \rightarrow H_2O - \text{sup} \quad (9)$$

$$H_2O + \text{sup} \rightarrow H_2O\text{–sup}$$

$$H_2O\text{--sup} \rightarrow OH\text{–sup} + H\text{–sup}$$

$$H\text{–sup} \rightarrow O\text{–sup} + H_2 + \text{sup}$$

Spill-over of oxygen species:

$$H - \text{sup} + * \rightarrow OH - * + \text{sup} \quad (11.a)$$

$$O - \text{up} + * \rightarrow O - * + \text{sup} \quad (11.b)$$

$$CH_X\text{–}*n + OH\text{–}* \rightarrow CO + (x+1)/2\,H_2 + (n+1)* \quad (12.a)$$

$$CH_X\text{–}*n + O\text{–}* \rightarrow CO + x/2\,H_2 + (n+1)* \quad (12.b)$$

$$CH_X\text{–}*n \rightarrow C\text{–}*n \rightarrow [Ni, C] \rightarrow \text{"whisker"} \quad \text{(whisker carbon)} \quad (13)$$

$$C\text{–}* \rightarrow \text{"gum"} \quad \text{(gum carbon)} \quad (14)$$

*: represents active sites; *2: represents adsorption sites acting at the same time and sup: indicates adsorption sites on support surface.

Therefore, the most important factors related to the catalyst structure influence on the activity of a steam reforming catalyst are metal area, metal particle size, metal–support interface length, support area and its ability to adsorb and activate water.

Designing a catalyst for preventing carbon formation [35] implies the synthesis of a material with a suitable combination of textural properties (dispersion, form and metallic particle size, specific area and proportion of different superficial metallic planes, support characteristics) to get recombination of C_1 species with oxygen species coming from the water dissociation (reaction (12)) at the same rate at which they have been formed from C-Cα-scission (reaction (8)), and thus to avoid C_1 species remaining on active sites sufficient time to form coke.

In a previous work [35] we have studied nickel content influence on catalytic properties of several materials. Catalysts with low nickel content show stronger metal–support interaction, greater nickel dispersion, lower nickel particle size, greater support surface area, greater magnesium content (which leads to a higher capacity for water adsorption-dissociation and oxygen species mobility). All these characteristics produce materials with better resistance to carbon deposition. In Fig. 1 is shown intrinsic activity for samples studied in the previous work. We can observe that the optimum nickel content is 20%. In Fig. 2 we can see nickel content effect on carbon resistance. This figure shows carbon content on samples after 8 h reaction versus nickel content. Carbon content deposited during reaction is greater for samples with higher nickel content. Catalysts with higher nickel content favour reaction (8) more than oxygen species mobility, and catalysts with lower nickel content facilitate oxygen species mobility more than reaction (8). Catalysts with low nickel content could be promoted with several elements in order to improve their activity. In the same manner, catalysts with high nickel content could be promoted in order to improve their resistance to carbon deposition.

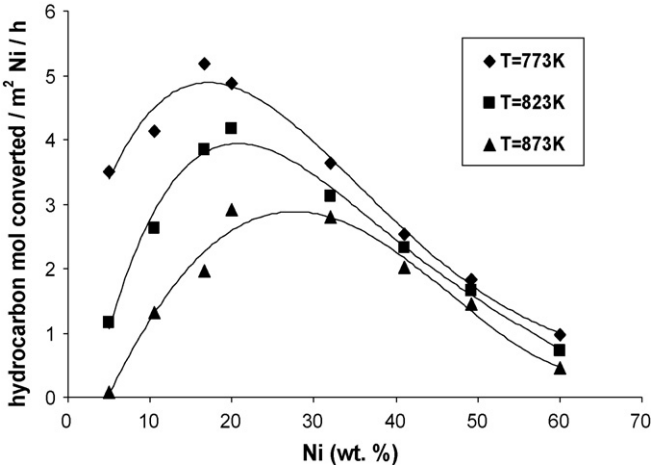

Fig. 1. Nickel content effect on intrinsic activity expressed per m^2 of nickel in the catalyst ($P = P_{atm}$, $W/F = 2\ g_{cat}{\cdot}h$/hydrocarbon mol, $S/C = 3H_2O$ mol/carbmon atom, $T = 823$ K, $G_{total}HSV = 225{,}160\ h^{-1}$).

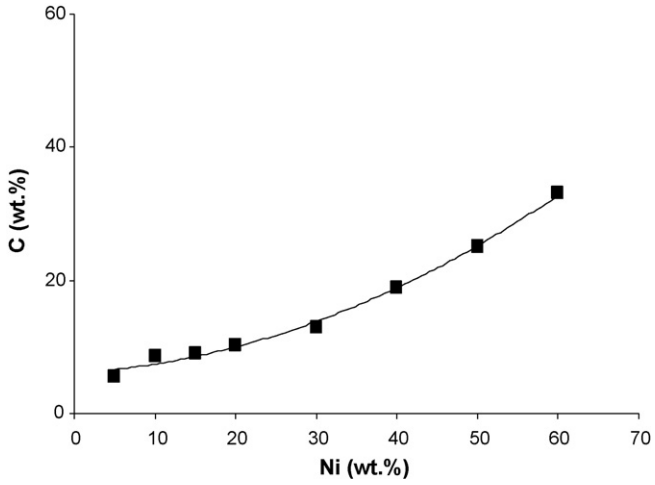

Fig. 2. Nickel content effect on carbon resistance. Carbon content of samples used in reaction during 8 h.

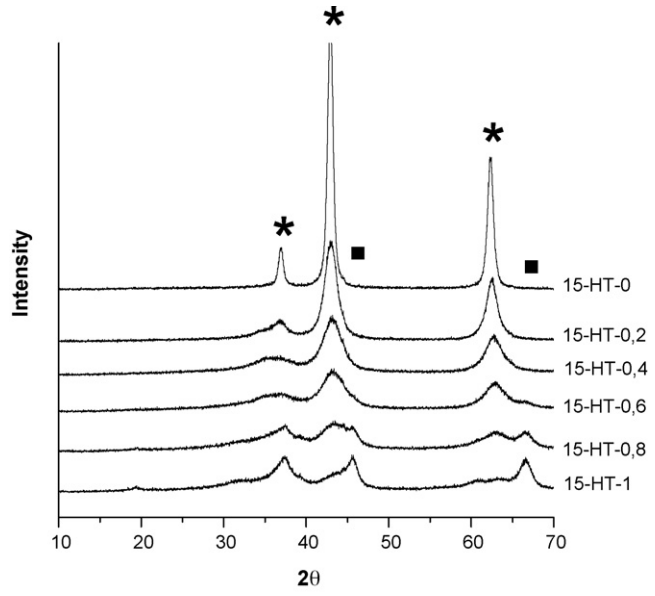

Fig. 3. X-ray diffraction of calcined samples for materials with different Al/Mg ratio ((*) peaks correspondent to mixed oxide phase and (■) peaks correspondent to alumina phase).

3.1. Aluminium/magnesium ratio influence

On Table 1 we can see nominal composition (wt.%) of samples prepared in order to study aluminium/magnesium ratio

Table 1
Composition (percentage in weight) for materials with different Al/Mg ratio

Sample	Percentage in weight (%)				Molar ratio	
	Ni	Mg	Al	O	Al(Al + Mg + Ni)	Al/(Al + Mg)
15-HT-0.0	15.2	51.0	0.0	33.8	0.00	0.00
15-HT-0.2	14.7	36.1	10.1	39.1	0.18	0.20
15-HT-0.4	15.0	27.5	20.1	37.5	0.35	0.40
15-HT-0.6	14.8	16.5	27.1	41.5	0.52	0.60
15-HT-0.8	15.3	8.3	37.2	39.2	0.70	0.80
15-HT-1.0	15.1	0.0	42.5	42.4	0.86	1.00

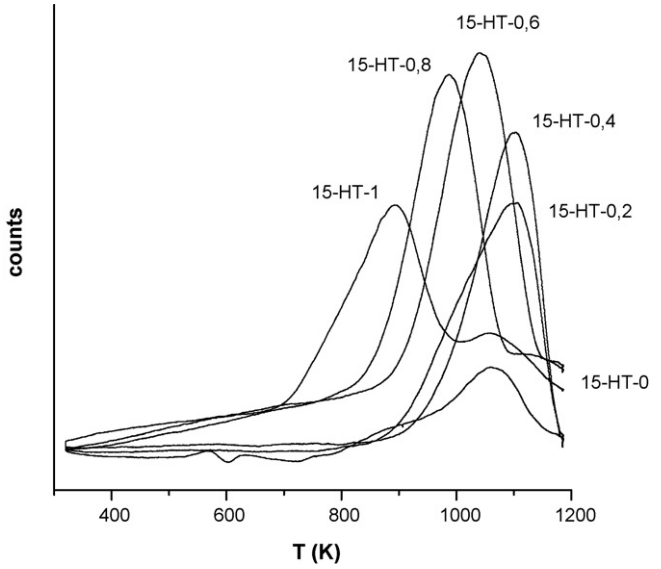

Fig. 4. Temperature programmed reduction (TPR) of calcined samples for materials with different Al/Mg ratio.

effect for different nickel content. In Figs. 3 and 4 appear characterization results correspondent to calcined samples prepared with different aluminium/magnesium ratio. Fig. 3 shows X-ray diffraction (XRD) pattern of calcined samples correspondent to the series 15-HT-*X*, in that figure we observe how peaks width decreases as magnesium content increases. In X-ray diffraction pattern correspondent to the material before calcination, only samples with Al/(Al + Mg) ratio between 0.2 and 0.4 showed peaks correspondent to layered double hydroxide structure, the other ones showed a mixture of phases. Fig. 4 shows TPR curves for calcined samples correspondent to the samples. From the metal–support interaction elucidated by temperature reduction shown in TPR curves we can conclude that thermal stability of Ni-Mg-Al materials increases with the increasing Mg/Al ratio, [34] until Al/(Al + Mg) ratio between 0.2 and 0.4, then decreases a little. On Table 2 we can see how nickel reduction temperature increases with magnesium content until a determined value since it reduction temperature decreases, indicating stronger interaction with the support when greater is the magnesium content, showing a maximum for Al/(Al + Mg) ratio between 0.2 and 0.4. Finally, the same table, shows how specific surface area increases with aluminium content, showing a maximum for Al/(Al + Mg) ratio 0.8.

Table 2
BET area and nickel reduction temperature for materials with different Al/Mg ratio

Sample	BET area (m^2/g_{cat})	$T_{max\ red}$ (K)
15-HT-0.0	99	1055
15-HT-0.2	196	1083
15-HT-0.4	234	1091
15-HT-0.6	256	1023
15-HT-0.8	295	970
15-HT-1.0	287	883

Table 3
Estimated nickel particle size, nickel dispersion, reduction degree and nickel active area for materials with different Al/Mg ratio

Sample	d_{Ni} (nm)	Dispersion (%)	Reduction degree (%)	Active area (m^2_{Ni}/g_{cat})
15-HT-0.0	12.0	8.1	61	4.3
15-HT-0.2	10.4	9.3	60	4.9
15-HT-0.4	10.7	9.1	63	5.0
15-HT-0.6	12.0	8.1	67	4.7
15-HT-0.8	15.0	6.5	80	4.5
15-HT-1.0	19.7	4.9	98	4.2

Table 4
Estimated nickel particle size, nickel dispersion, reduction degree and nickel active area for materials reduced with different temperature

Sample	d_{Ni} (nm)	Dispersion (%)	Reduction degree (%)	Active area (m^2_{Ni}/g_{cat})
15-HT-r773	9.8	9.9	43	3.7
15-HT-r873	10.1	9.6	52	4.4
15-HT-r973	10.4	9.3	60	4.9
15-HT-r1073	11.9	8.2	67	4.7

Reduced samples characterization results are presented on Table 3. In this table we can see how nickel particles size increases with aluminium content. This table we can observe that nickel dispersion shows a maximum between Al/(Al + Mg) = 0.2–0.4. Reduction degree reached for different samples after the same activation treatment is shown in this table too. Reduction degree increases with aluminium content due to the minor interaction degree of nickel with aluminium support. Finally, we can see how nickel active area shows a maximum between 0.2 and 0.4 Al/(Al + Mg) ratio.

Therefore, Al/(Al + Mg) ratio between 0.2 and 0.4 seems to be the best proportion to obtain the optimum textural properties of the material. We have to remark the benefits of layered double hydroxide structure formation during catalysts synthesis.

In Fig. 5 we can see aluminium/magnesium ratio effect on catalytic activity. This figure shows a maximum of nickel intrinsic activity for Al/(Al + Mg) ratio between 0.2 and 0.4. This proportion seems to combine the best textural properties and nickel dispersion, as we have concluded on Table 3, in this table we have seen a maximum on nickel dispersion and on nickel active area for this Al/(Al + Mg) ratio.

In Fig. 6 we can see aluminium/magnesium ratio effect on carbon resistance, carbon resistance increases with magnesium content due to the basicity provided for magnesium support. The support and its properties seemed to play a key role in the performance of the layered double hydroxide-derived catalysts. Increasing magnesium content we obtain stronger metal–support interaction, and increasing aluminium content we obtain greater specific surface area. Therefore, there is an optimum magnesium/aluminium ratio. We can relation carbon resistance with nickel particle size shown on Table 3.

3.2. Reduction temperature influence

Base catalyst has been reduced with different reduction temperature in order to study reduction temperature influence

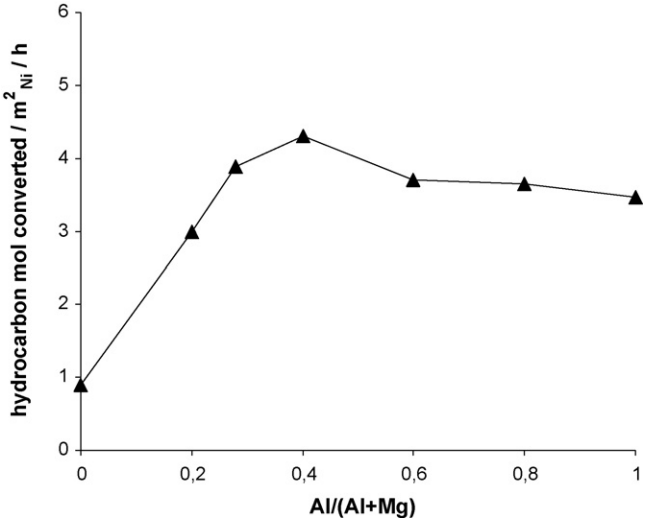

Fig. 5. Aluminium/magnesium ratio effect on intrinsic activity ($P = P_{atm}$, $W/F = 2\ g_{cat}$·h/hydrocarbon mol, $S/C = 3H_2O$ mol/carbon atom, $T = 823$ K, $G_{total}HSV = 225{,}160\ h^{-1}$).

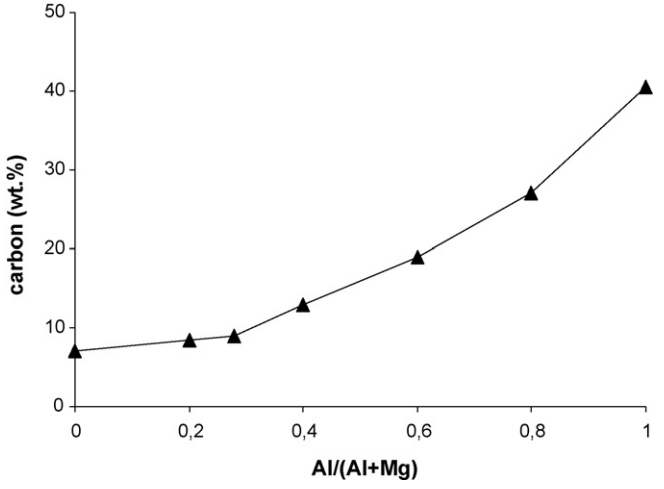

Fig. 6. Aluminium/magnesium ratio effect on carbon resistance. Carbon content of samples used in reaction during 8 h.

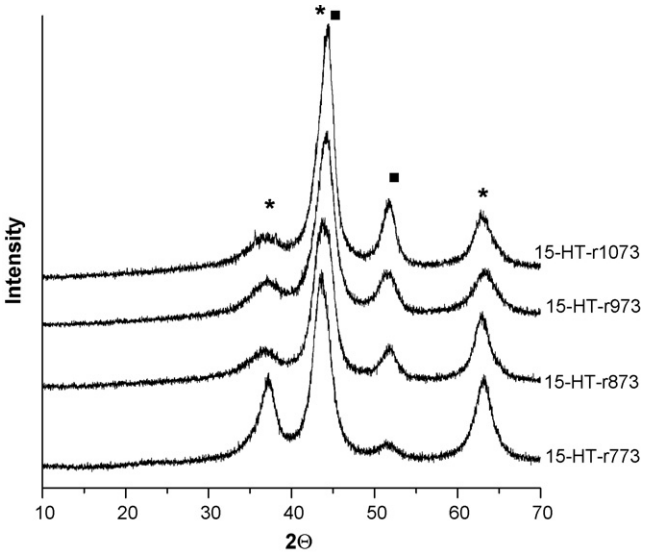

Fig. 7. X-ray diffraction of reduced samples for materials reduced with different temperature ((*) peaks correspondent to mixed oxide phase and (■) peaks correspondent to metallic nickel).

on catalyst structure and activity. Table 4 shows characterization results of reduced samples by different reduction temperature. In Fig. 7 we can see X-rays diffraction patterns corresponding to reduced samples of the series 15-HT-r*X*. Intensity correspondent to nickel oxide phase diminishes and the one correspondent to nickel metallic phase increases as the reduction temperature increases. On Table 4 we can see how nickel particle size increases, and nickel dispersion decreases, with reduction temperature. It would be due to the sintering phenomena acting at high temperatures. And, as it is expected, reduction degree increases with reduction temperature. Nickel active area increases with reduction temperature due to the increase observed on the reduction degree, but then it decreases due to the nickel particle size increases.

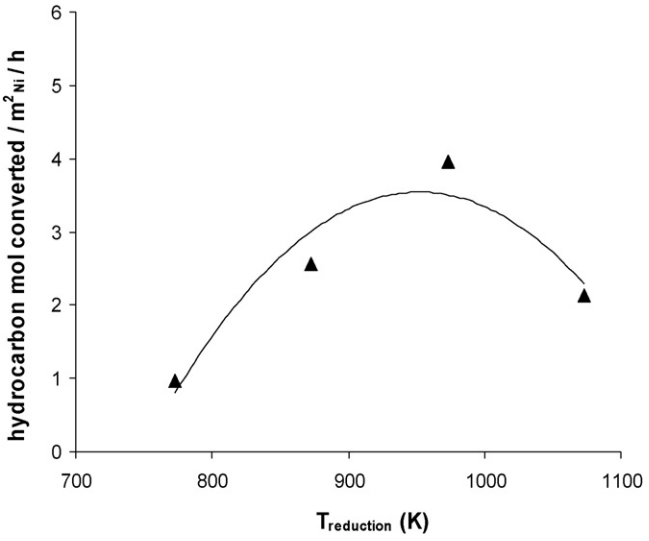

Fig. 8. Reduction temperature effect on intrinsic activity ($P = P_{atm}$, $W/F = 2$ g_{cat}·h/hydrocarbon mol, $S/C = 3H_2O$ mol/carbon atom, $T = 823$ K, $G_{total}HSV = 225{,}160$ h^{-1}).

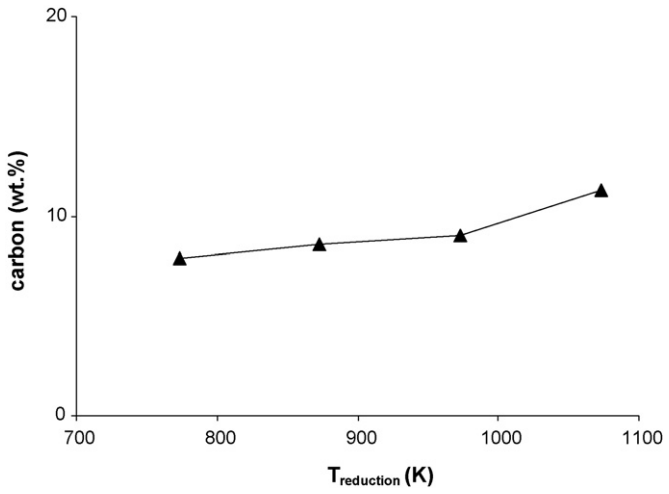

Fig. 9. Reduction temperature effect on carbon resistance. Carbon content of samples used in reaction during 8 h.

In Fig. 8 we can see reduction temperature effect on nickel intrinsic activity. This figure shows a maximum, nickel intrinsic activity increases with reduction temperature until a value, greater reduction temperatures does not offer greater activity since it produces sintering of metallic nickel particles as we have seen on Table 4.

In Fig. 9 we can see reduction temperature effect on carbon resistance. It decreases with reduction temperature due to the nickel particle size increment.

Increasing reduction temperature produces an increase on nickel active area (Fig. 10), but metallic nickel particles size increase too (Fig. 7), offering an increase on activity (until a determined reduction temperature) but a decrease on carbon resistance. Optimum reduction temperature is dependent of the reducibility of the calcined materials, rationed with the metal–support interaction.

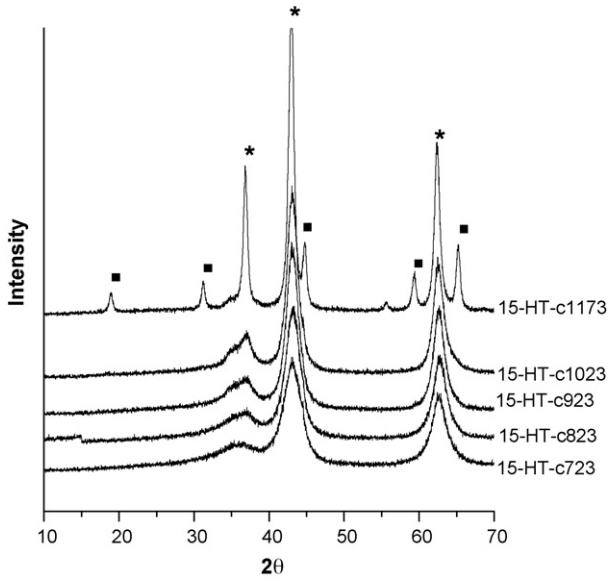

Fig. 10. X-ray diffraction of calcined samples for materials calcined at different temperature ((*) peaks correspondent to mixed oxide phase and ((■) peaks correspondent to NiMgAl espinela phase).

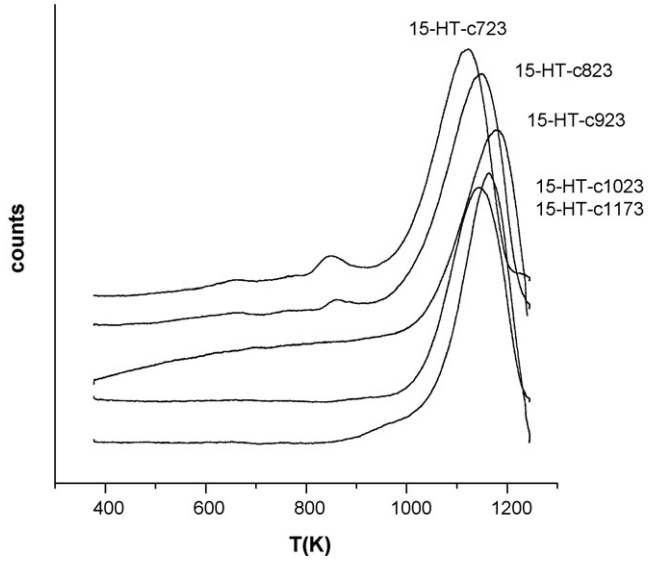

Fig. 11. Temperature programmed reduction (TPR) of calcined samples for materials calcined at different temperature.

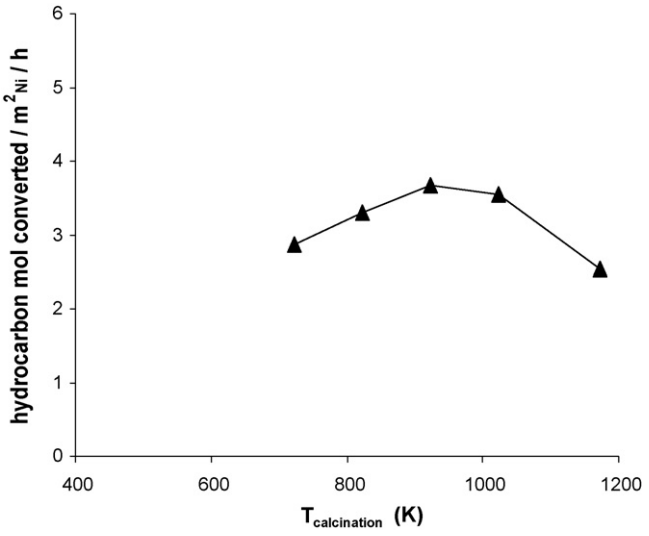

Fig. 12. Calcination temperature effect on intrinsic activity. ($P = P_{atm}$, $W/F = 2$ g_{cat}·h/hydrocarbon mol, $S/C = 3H_2O$ mol/carbon atom, $T = 823$ K, $G_{total}HSV = 225{,}160$ h^{-1}).

Table 5
BET area for materials calcined at different temperature

Sample	BET area (m^2/g_{cat})	$T_{max\ red}$ (K)
15-HT-c723	293	1020
15-HT-c823	265	1070
15-HT-c923	234	1083
15-HT-c1023	180	1095
15-HT-c1173	95	1094

3.3. Calcination temperature influence

Base catalyst has been calcined at different temperatures in order to study the influence of this variable on catalyst structure and activity. Figs. 10 and 11 show the characterization results for samples prepared at different calcination temperatures. Fig. 10 shows X-ray diffraction pattern of calcined samples correspondent to the series 15-HT-c*X*, in that figure we observe how peak width decreases as calcination temperature increases, so NiO particle size increased with increasing calcination temperature. Fig. 11 shows TPR curves for samples of 15-HT-c*X* series, we can see how the maximum of reduction temperature increases with calcination temperature until a determined value, further calcination temperature do not produce significant changes in the metal–support interaction. Finally on Table 5 is shown BET area and nickel reduction temperature values. BET area increases with calcination temperature, then reaches a maximum and finally decreases with increasing calcination temperature. This result can be explained due to the sintering of sample. Nickel reduction temperature increases with calcination temperature, as we have seen on Fig. 11, reaching a limit value at 923 K.

Table 6 shows the reduced samples characterization results. Nickel particle size increases with calcination temperature like NiO particle size is also greater with the calcination temperature, as we have seen in Fig. 10. Therefore, nickel dispersion decreases with calcination temperature in the same sense in which nickel particle size increases. Reduction degree decreases with calcination temperature, reaching a limit value associated this fact with the metal–support interaction shown in Fig. 11, and nickel reduction temperature shown on Table 5. Finally, nickel active area increases with calcination temperature, reaches a maximum and then decreases with calcination temperature due to the metal particle size increases, the nickel dispersion decreases and the BET area decreases.

In Fig. 12 we can see the calcination temperature effect on activity. First, nickel intrinsic activity increases due to the increase of the BET area (Table 5) and the nickel active area (Table 6), then it reaches a maximum and finally it decreases with calcination temperature associated with the decrease in the nickel active area and dispersion.

In Fig. 13 we can see the calcination temperature effect on carbon resistance. Carbon resistance decreases with calcination temperature associated with the decrease in the nickel active area and dispersion and the increase of nickel particle size.

Table 6
Estimated nickel particle size, nickel dispersion, reduction degree and nickel active area for materials calcined at different temperature

Sample	d_{Ni} (nm)	Dispersion (%)	Reduction degree (%)	Active area (m^2_{Ni}/g_{cat})
15-HT-c723	9.5	10.2	80	7.1
15-HT-c823	9.8	9.9	70	6.0
15-HT-c923	10.4	9.3	60	4.9
15-HT-c1023	11.4	8.5	55	4.1
15-HT-c1173	22.3	4.4	60	2.3

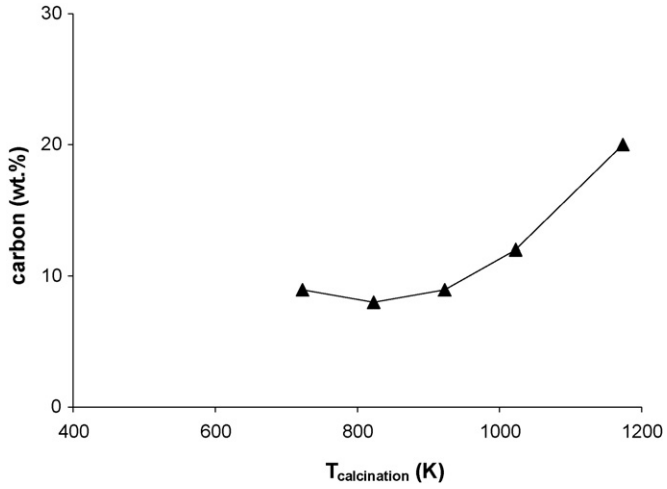

Fig. 13. Calcination temperature effect on carbon resistance. Carbon content of samples used in reaction during 8 h.

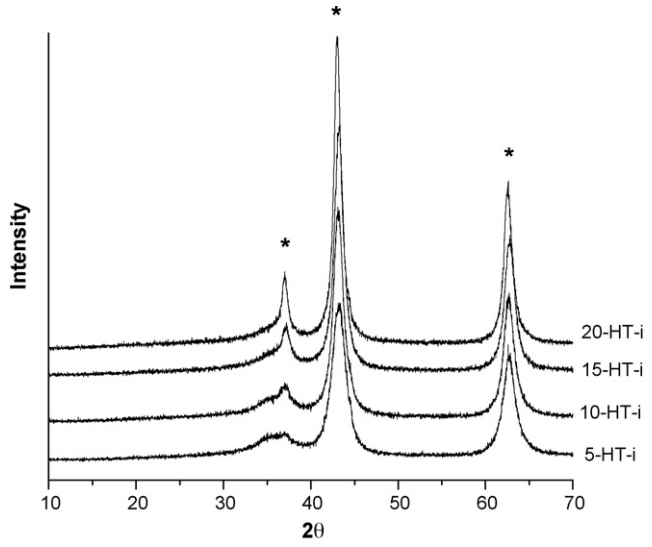

Fig. 14. X-ray diffraction of calcined samples for materials impregnated with different nickel content ((*) peaks correspondent to mixed oxide phase).

There is optimum calcination temperature for obtaining the maximum activity, increasing calcination temperature produces a decrease on nickel active area and an increase on nickel particle size, offering a decrease on activity and on carbon resistance.

3.4. Nickel incorporation method influence

We have studied the influence of nickel incorporation method comparing samples prepared by precipitation [35] and by impregnation methods.

Table 7
Composition (wt.%) for materials impregnated with different nickel content

Sample	d_{Ni} (nm)	Dispersion (%)	Reduction degree (%)	Active area (m^2_{Ni}/g_{cat})
5-HT-i	12.6	7.7	63	1.4
10-HT-i	15.8	6.1	72	2.6
15-HT-i	18.6	5.2	83	3.8
20-HT-i	21.8	4.5	96	4.9

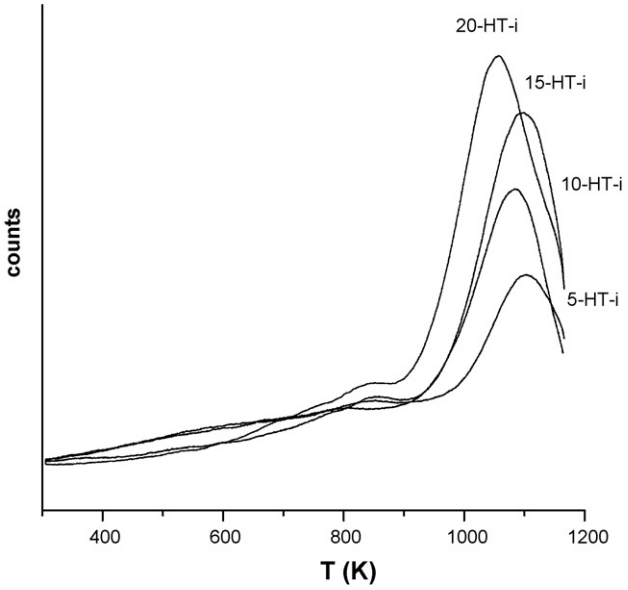

Fig. 15. Temperature programmed reduction (TPR) of calcined samples for materials impregnated with different nickel content.

In Table 7 we can see the composition of calcined samples prepared by impregnation method and Fig. 14 shows X-ray diffraction pattern of these samples. If we compare the peak width for samples prepared by impregnation and precipitation, we can observe that this is greater for samples prepared by precipitation method [35]. Fig. 15 shows the curves of temperature programmed reduction correspondent to samples obtained by impregnation method. Nickel oxide is less reducible when nickel content decreases, this result gives us a qualitative measurement of nickel dispersion, since the most dispersed particles show stronger interaction with the support and usually they are less reducible.

In Table 7 is shown the nickel reduction temperature for samples obtained by impregnation method. We can see, in this figure, how nickel reduction temperature diminishes as nickel content increases. These values are lower that the corresponding samples prepared by precipitation [35] indicating greater interaction metal–support on samples prepared by this method. Finally, in this table is shown BET area, and it diminishes with nickel content and it is greater for samples prepared by precipitation method.

This series of catalysts has also been characterized after reduction treatment (Table 8). We can observe, in this table that nickel particle size increases with nickel content and it is smaller for those samples prepared by precipitation method. Nickel dispersion and reduction degree follow the logical tendency. Finally, we can observe how nickel active area increases with nickel content and is greater for those samples prepared by precipitation method.

Precipitation method for introducing nickel results in stronger metal–support interaction than impregnation method. By precipitation method we can produce, in a single stage, more favourable catalyst structure for obtaining highly and finely dispersed nickel particles than by impregnation one.

Table 8
Estimated nickel particle size, nickel dispersion, reduction degree and nickel active area for materials impregnated with different nickel content

Sample	Percentage in weight (%)				Molar ratio		BET area (m^2/g_{cat})	$T_{max\ red}$ (K)
	Ni	Mg	Al	O	Al(Al + Mg + Ni)	Al/(Al + Mg)		
5-HT-i	5.0	29.5	10.9	54.6	0.24	0.25	213	1094
10-HT-i	10.0	28.0	10.3	51.7	0.23	0.25	180	1090
15-HT-i	15.0	26.4	9.7	48.8	0.21	0.25	152	1084
20-HT-i	20.0	24.9	9.2	45.9	0.20	0.25	151	1058

In Fig. 16 we can see nickel incorporation method effect on catalytic activity, the catalysts prepared by precipitation method showed higher nickel intrinsic activity than those prepared by impregnation method, being the difference most intense when greater is the nickel content on the samples. It is due to higher nickel active area offered by these samples.

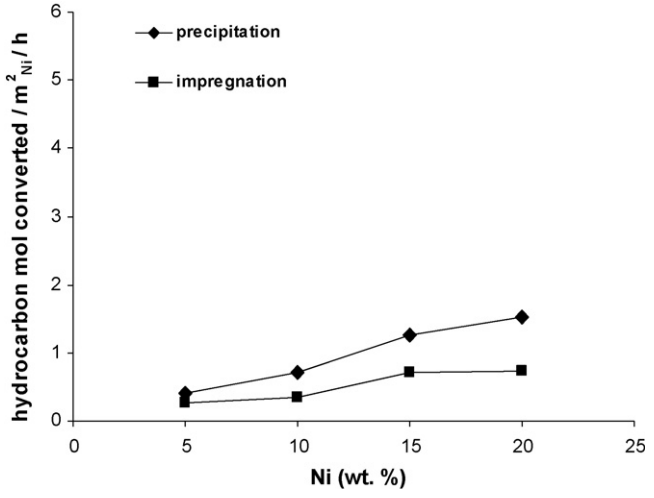

Fig. 16. Nickel incorporation method effect on intrinsic activity. ($P = P_{atm}$, $W/F = 2\ g_{cat}$·h/hydrocarbon mol, $S/C = 3H_2O$ mol/carbon atom, $T = 828$ K, G_{total}HSV = 225,160 h^{-1}).

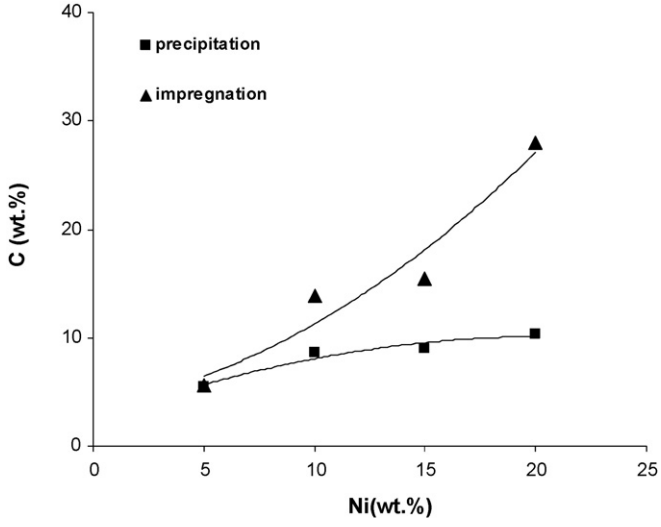

Fig. 17. Nickel incorporation method effect on carbon resistance. Carbon content of samples used in reaction during 8 h.

In Fig. 17 we can see the nickel incorporation method effect on carbon resistance. Similar to the activity, samples obtained by precipitation method showed better resistance to carbon deposition than those prepared by impregnation, being the difference most intense when greater is the nickel content on the samples. It is due to smaller nickel particle size obtained on samples prepared by precipitation method.

Catalyst performance is strongly related to the nickel particle size. The smaller the Ni particle size, the resistance to carbon deposition is enhanced. Large nickel crystallites favour the adsorption of hydrocarbon (reactions (7) and (8)) respect to the recombination with oxygen species (reactions (12)). Then, the reactions forming carbon deposition as reactions (13) and (14) are favoured leading to a severe catalyst deactivation [35].

4. Conclusions

Catalysts obtained by calcination/reduction of layered double hydroxide-type materials characterized by highly dispersed metallic crystallites stabilized inside a matrix with high surface area, are suitable materials in naphtha steam reforming reaction.

Synthesis parameters such as method of introduction of active species, amount of components and thermal treatments (calcination and reduction), could be optimized to obtain a material which presents high catalytic activity and high resistance to carbon formation. This material must contain the adequate combination of the textural properties, the most important factors related to the catalysts structure influence on the activity and carbon resistance of a steam reforming catalysts are metal area, metal particle size, metal–support interface length, support area and its ability to adsorb water.

Increasing nickel content produces an increase on nickel active area, but metallic nickel particles size increase too, offering an increase on activity (until a determined nickel content) but a decrease on carbon resistance.

The support and its properties seemed to play a key role in the performance of the HT-derived catalysts. Increasing magnesium content we obtain stronger metal–support interaction, and increasing aluminium content we obtain greater specific surface area. Therefore, there is an optimum aluminium/magnesium ratio (Al/(Al + Mg) = 0.2–0.4).

Calcination temperature must be great enough to obtain sufficient interaction degree but not too high in order to avoid catalyst sintering.

Increasing reduction temperature produces an increase on nickel active area, but metallic nickel particles size increase

too, offering an increase on activity (until a determined reduction temperature) but a decrease on carbon resistance.

Nickel incorporation by precipitation method offers more highly and finely dispersed nickel particles than incorporation by impregnation method.

Synthesis parameters have an important influence on metal–support interaction, when stronger are metal–support interactions more favourable is catalyst structure for obtaining better catalysts. Catalyst performance is strongly related to the nickel particle size and to the support and its properties.

Acknowledgements

We are thankful to the Generalitat Valenciana by its aid in the financing I + D (CTIDIB/2002/20) project. N. Morlanés thanks for to the Ministry of Science and Technology by the concession of a predoctoral scholarship (I3P/2001).

References

[1] J. Quakernat, Int. J. Hydrogen Energy 20 (1995) 485.
[2] A. Naidja, et al. Prog. Energy Comb. Sci. 29 (2003) 155.
[3] P. Ferreira Aparicio, M.J. Benito, Catal. Rev. 47 (2005) 491.
[4] S. Natesakhawat, Thesis, The Ohio State University, 2005.
[5] Y.S. Seo, A. Shirley, S.T. Kolaczkowski, J. Power Sources 108 (2002) 213.
[6] M. Krumplet, R. Rumar, K.M. Myles, J. Power Sources 49 (1994) 37.
[7] Ross A. Lemons, J. Power Sources 29 (1990) 251.
[8] National Energy Technology Laboratory from U.S. Department of Energy, Fuel Cell Handbook by EG&G Services Parsons, Inc. Science Applications International Corporation, fifth ed., 2000.
[9] V.A. Antonuci, A.S. Arico, J. Power Sources 62 (1996) 95.
[10] K. Kaneda, et al. Catal. Surv. Japan 4 (2000) 31.
[11] C. Flego, Appl. Catal. A: Gen. 270 (2004) 113.
[12] D.L. Trimm, et al. Catal. Today 93–95 (2004) 17.
[13] X. Wang, R.J. Gorte, Appl. Catal. A: Gen. 224 (2002) 209.
[14] Q. Ming, T. Healey, L. Allen, P. Irving, Catal. Today 77 (2002) 51.
[15] J.R. Rostrup-Nielsen, Catalysis science and technology, in: J.R. Anderson, M. Bouduart (Eds.), Catalytic Steam Reforming, vol. 5, Springer-Verlag editions, 1984 (Chapter 1).
[16] J.R. Rostrup Nielsen, J. Sehested, Adv. Catal. 47 (2002) 65.
[17] J.R. Rostrup Nielsen, Stud. Surf. Sci. Catal. 139 (2001) 1.
[18] J.R. Rostrup Nielsen, J. Catal. 209 (2002) 365.
[19] J.N. Armor, Appl. Catal. A: Gen. 176 (1999) 159.
[20] M.A. Peña, et al. Appl. Catal. A: Gen. 144 (1996) 7.
[21] J. Zhang, et al. Int. J. Hydrogen Energy 26 (2001) 795.
[22] J. Zhang, et al. Appl. Catal. A: Gen. 243 (2003) 251.
[23] D. Tichit, B. Coq, Cattech 7 (2003) 206.
[24] A. Bhattacharyya, V.W. Chang, D.J. Schumacher, Appl. Clay Sci. 13 (1998) 317.
[25] Y. Zhang, G. Xiong, S. Sheng, W. Yang, Catal. Today 63 (2000) 517.
[26] F. Arena, B.A. Horrell, D.L. Cocke, A. Parmaliana, N. Giordano, J. Catal. 132 (1991) 58.
[27] A. Parmaliana, F. Arena, F. Frusteri, S. Coluccia, L. Marchese, G. Martra, A.L. Chuvilin, J. Catal. 141 (1993) 34.
[28] F. Cavani, F. Trifiro, A. Vaccari, Catal. Today 11 (1991) 2.
[29] A. Vaccari, Appl. Clay Sci. 14 (1999) 161.
[30] T. Borowieki, Appl. Catal. A: Gen. 4 (1987) 207.
[31] A. Velty, Thesis, Valencia University, 2003.
[32] B.D. Cullity, Elements of X-Ray Diffraction, Addision-Wesley, London, 1978.
[33] T. Borowieki, Appl. Catal. A: Gen. 4 (1982) 223.
[34] T. Borowieki, Appl. Catal. A: Gen. 4 (1984) 273.
[35] F. Melo, N. Morlanés, Catal. Today 107–108 (2005) 458.